



OPEN

SUBJECT AREAS:

FUEL CELLS

ELECTROCHEMISTRY

ELECTRONIC DEVICES

MATERIALS SCIENCE

# Highly efficient and robust cathode materials for low-temperature solid oxide fuel cells: $\text{PrBa}_{0.5}\text{Sr}_{0.5}\text{Co}_{2-x}\text{Fe}_x\text{O}_{5+\delta}$

Sihyuk Choi<sup>1</sup>, Seonyoung Yoo<sup>1</sup>, Jiyoun Kim<sup>1,2</sup>, Seonhye Park<sup>1</sup>, Areum Jun<sup>1</sup>, Sivaprakash Sengodan<sup>1</sup>, Junyoung Kim<sup>1</sup>, Jeeyoung Shin<sup>3</sup>, Hu Young Jeong<sup>4</sup>, YongMan Choi<sup>5</sup>, Guntae Kim<sup>1</sup> & Meilin Liu<sup>1,6</sup>

Received  
18 March 2013

Accepted  
26 July 2013

Published  
15 August 2013

Correspondence and requests for materials should be addressed to G.K. (gkim@unist.ac.kr) or M.L.L. (meilin.liu@mse.gatech.edu)

<sup>1</sup>Interdisciplinary School of Green Energy, Ulsan National Institute of Science and Technology (UNIST), Ulsan, 689–798, Korea, <sup>2</sup>Convergence Technology Research Directorate, Agency for Defence Development, Daejeon, Republic of Korea, <sup>3</sup>Department of Mechanical Engineering, Dong-Eui University, Busan 614–714, Korea, <sup>4</sup>UNIST Central Research Facilities and School of Mechanical and Advanced Materials Engineering, UNIST, Ulsan, 689–798, Korea, <sup>5</sup>SABIC Technology Center, Riyadh, 11551, Saudi Arabia, <sup>6</sup>School of Materials Science and Engineering, Center for Innovative Fuel Cell and Battery Technologies, Georgia Institute of Technology, Atlanta, GA 30332-0245, USA.

Solid oxide fuel cells (SOFC) are the cleanest, most efficient, and cost-effective option for direct conversion to electricity of a wide variety of fuels. While significant progress has been made in anode materials with enhanced tolerance to coking and contaminant poisoning, cathodic polarization still contributes considerably to energy loss, more so at lower operating temperatures. Here we report a synergistic effect of co-doping in a cation-ordered double-perovskite material,  $\text{PrBa}_{0.5}\text{Sr}_{0.5}\text{Co}_{2-x}\text{Fe}_x\text{O}_{5+\delta}$ , which has created pore channels that dramatically enhance oxygen ion diffusion and surface oxygen exchange while maintaining excellent compatibility and stability under operating conditions. Test cells based on these cathode materials demonstrate peak power densities  $\sim 2.2 \text{ W cm}^{-2}$  at  $600^\circ\text{C}$ , representing an important step toward commercially viable SOFC technologies.

The demand for clean and sustainable energy has stimulated great interest in fuel cells, which allows direct conversion of chemical fuels to electricity. Among all types of fuel cells, solid oxide fuel cells (SOFCs) have the potential to offer the highest energy efficiency and excellent fuel flexibility<sup>1–9</sup>. To make SOFC technology affordable, however, the operating temperature must be further reduced so that much less expensive materials may be used for other cell components and balance of plant<sup>5</sup>. Unfortunately, SOFC performance decreases rapidly as the operating temperature is reduced, especially the cathode for oxygen reduction reaction (ORR)<sup>10,11</sup>. While  $\text{La}_{1-x}\text{Sr}_x\text{MnO}_3$  (LSM) is widely used as the cathode material for yttria-stabilized zirconia (YSZ)-based SOFCs because of its excellent compatibility with YSZ electrolyte and other cell components; the cathodic polarization loss at lower temperatures is unacceptable. Accordingly, extensive efforts have been devoted to the search for more active cathode materials toward ORR at lower temperatures.

In particular, mixed conducting oxides with simple perovskite structure have been studied as alternative cathode materials for intermediate-temperature (IT)-SOFCs, including  $\text{Sm}_{0.5}\text{Sr}_{0.5}\text{CoO}_{3-\delta}$  (SSC)<sup>12</sup>,  $\text{Ba}_{0.5}\text{Sr}_{0.5}\text{Co}_{0.8}\text{Fe}_{0.2}\text{O}_{3-\delta}$  (BSCF)<sup>13</sup>, and  $\text{La}_{0.6}\text{Sr}_{0.4}\text{Co}_{1-x}\text{Fe}_x\text{O}_{3-\delta}$  (LSCF)<sup>14</sup>. Among them, BSCF was reported to have very low area-specific resistance (ASR), about  $0.05 \sim 0.08 \Omega \text{ cm}^2$  at  $600^\circ\text{C}$ . However, its applicability to commercial fuel cells is hindered by its limited compatibility with other cell components and long-term stability.

Recently, cation-ordered double-perovskite structures such as  $\text{LnBaCo}_2\text{O}_{5+\delta}$  (Ln = Pr, Nd, Sm, and Gd) have attracted much attention due to their easier oxygen ion diffusion, faster surface oxygen exchange, and higher electrical conductivity at lower temperatures than simple perovskite cathode materials<sup>15–17</sup>, as corroborated by electrical conductivity relaxation (ECR)<sup>15</sup> and ion exchange depth profile (IEDP)<sup>17,18</sup> studies. This family of double perovskite compounds have a general formula of  $\text{AA}'\text{B}_2\text{O}_{5+\delta}$ , where  $\text{A} = \text{Y}$  or a trivalent lanthanide ion,  $\text{A}' = \text{Ba}$  or  $\text{Sr}$ , and  $\text{B}$  is a first row transition metal ion or a mixture of them. These compounds have a layered structure with a stacking sequence of  $\dots[\text{A}'\text{O}][\text{BO}_2][\text{AO}_\delta][\text{BO}_2]\dots$ , similar to the structure of the cuprate superconductors. The vacant sites are arranged so that the coordination number for A cation is eight when  $\delta = 0$ . All oxygen vacancies are confined only to the  $\text{LnO}$  plane, and so is oxygen migration<sup>18</sup>. The high concentration of mobile oxygen species may be responsible for the high diffusivity of oxide ions in the bulk and the enhanced surface activity toward ORR<sup>15</sup>.



Some interesting effects of ion substitution on the properties of  $\text{LnBaCo}_2\text{O}_{5+\delta}$  have been reported<sup>19–21</sup>. For example, the replacement of Pr by Gd was reported to diminish the concentration of oxygen defects, the electrical conductivity, and the performance as a cathode in a fuel cell<sup>19</sup>. On the other hand, a reverse trend was found for the substitution of Ba by Sr in the same material<sup>20</sup>. Further, various transition metal ions have been introduced into the B-site, including Fe, Cu, and Ni. As Co is substituted by Fe, the thermal expansion coefficient (TEC) and electronic conductivity decreased; however, the oxygen ion diffusivity, ORR activity, and stability increased. Thus, the properties can be tailored by the type and the amount of proper ion substitution.

Here we report a synergistic effect of co-doping (Sr on A-site and Fe on B-site) in a cation-ordered double-perovskite,  $\text{LnBaCo}_2\text{O}_{5+\delta}$ , to create crystalline channels for fast oxygen ion diffusion and rapid surface oxygen exchange while maintaining the compatibility with the electrolytes for IT-SOFCs and the durability under operating conditions.

## Results

**Characterization of  $\text{PrBa}_{0.5}\text{Sr}_{0.5}\text{Co}_{2-x}\text{Fe}_x\text{O}_{5+\delta}$  ( $x = 0, 0.5$ , and  $1.0$ ).** X-ray diffraction (XRD) analysis of Fe-doped  $\text{PrBa}_{0.5}\text{Sr}_{0.5}\text{Co}_{2-x}\text{Fe}_x\text{O}_{5+\delta}$  ( $x = 0, 0.5$ , and  $1.0$ ) samples suggests that they had a single phase without detectible amount of impurity after firing at  $1100 \sim 1150^\circ\text{C}$  in air for 12 hours (Supplementary Fig. S1a). Rietveld analysis of the XRD data indicates that the  $\text{PrBa}_{0.5}\text{Sr}_{0.5}\text{Co}_{1.5}\text{Fe}_{0.5}\text{O}_{5+\delta}$  (PBSCF05) compound has a tetragonal structure ( $P4/mmm$ ) with  $a = 3.871 \text{ \AA}$  and  $c = 7.757 \text{ \AA}$  (Supplementary Fig. S1c). The lattice expands with increasing Fe content as the smaller  $\text{Co}^{3+}$  ( $r = 0.545 \text{ \AA}$ ) or  $\text{Co}^{4+}$  ( $r = 0.530 \text{ \AA}$ ) ions are replaced

by the larger  $\text{Fe}^{3+}$  ( $r = 0.645 \text{ \AA}$ ) or  $\text{Fe}^{4+}$  ( $r = 0.585 \text{ \AA}$ ) ions (Supplementary Table S1). As temperature increased from room temperature to operating temperature, the cell volume was expanded, but the structure ( $P4/mmm$ ) remains the same (Supplementary Fig. S2 and Supplementary Table S2).

Transmission electron microscopy (TEM) analyses (Fig. 1) of the as-synthesized and the annealed ( $700^\circ\text{C}$  for 600 hours) PBSCF05 sample suggest that the tetragonal structure has lattice constants of  $a = 3.871 \text{ \AA}$  and  $c = 7.757 \text{ \AA}$ , similar to the XRD analysis (Supplementary Fig. S1a and Supplementary Table S1). Further, the high-resolution TEM image (Fig. 1b) also confirms the ordered stacking sequence  $[\text{Ba}(\text{Sr})\text{O}]-[\text{Co}(\text{Fe})\text{O}_2]-[\text{PrO}_\delta]-[\text{Co}(\text{Fe})\text{O}_2]-[\text{Ba}(\text{Sr})\text{O}_2]$  of the structure. In particular, this crystal structure demonstrated remarkable stability at high temperatures; the atomic structure of the surface remains unchanged after annealing at  $700^\circ\text{C}$  for 600 hours (Fig. 1c and Supplementary Fig. S4), in stark contrast to simple perovskite cathode materials such as BSCF or LSCF. The latter is much less stable; surface segregation of Sr-enriched phases or SrO has been observed under similar conditions<sup>14</sup>, leading to gradual degradation in performance. As a result, a surface coating must be applied to suppress surface phase segregation<sup>22</sup>.

**Electrical and redox properties.** The electrical conductivities of each sample at a given temperature (Fig. 2a) increased with increasing partial pressure of oxygen,  $p(\text{O}_2)$ , an indication of a typical  $p$ -type conductor. This is ideally suited for cathode application where electron holes are generated (or electrons are consumed) by the ORR. In general, the cathode experiences a lower  $p(\text{O}_2)$  under fuel cell operating conditions due to cathodic polarization<sup>23</sup>. Therefore, sufficient electrical conductivity at relatively low  $p(\text{O}_2)$  is important to ensure efficient current collection and long-term stability. For all

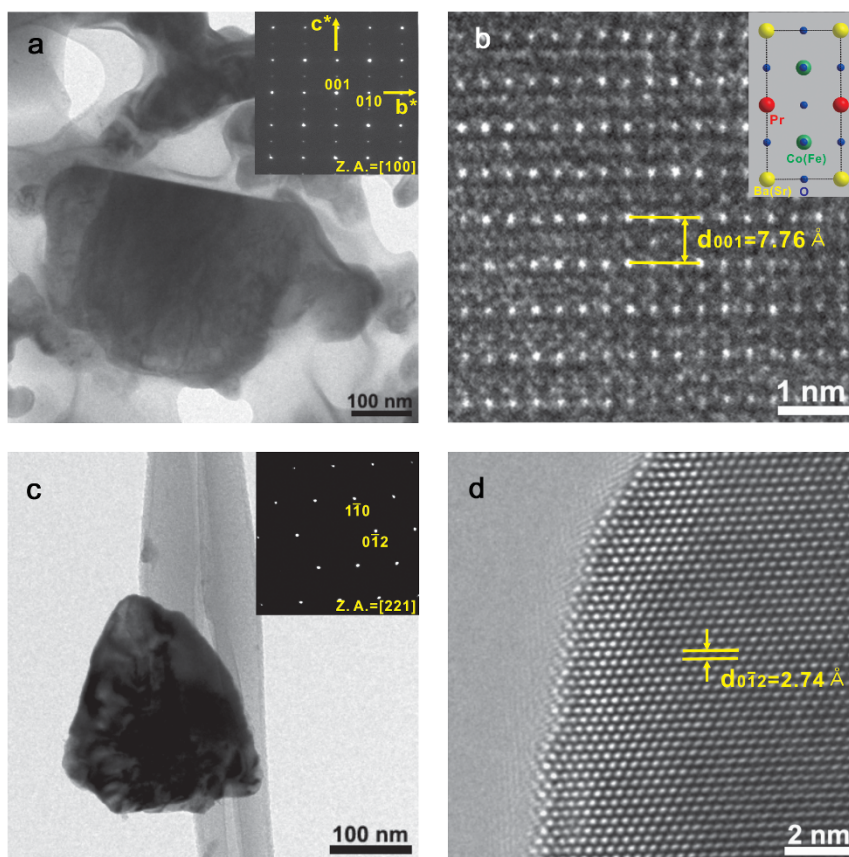


**Figure 1** | Transmission electron microscopy (TEM) analysis (a) A bright-field (BF) TEM image and an electron diffraction (ED) pattern obtained from an as-synthesized  $\text{PrBa}_{0.5}\text{Sr}_{0.5}\text{Co}_{2-x}\text{Fe}_x\text{O}_{5+\delta}$  sample. (b) A high-resolution TEM image of a grain in (a). (c) A BF-TEM image and an ED pattern of the sample annealed at  $700^\circ\text{C}$  for 600 hours. (d) A high-resolution TEM image of a grain after annealing.

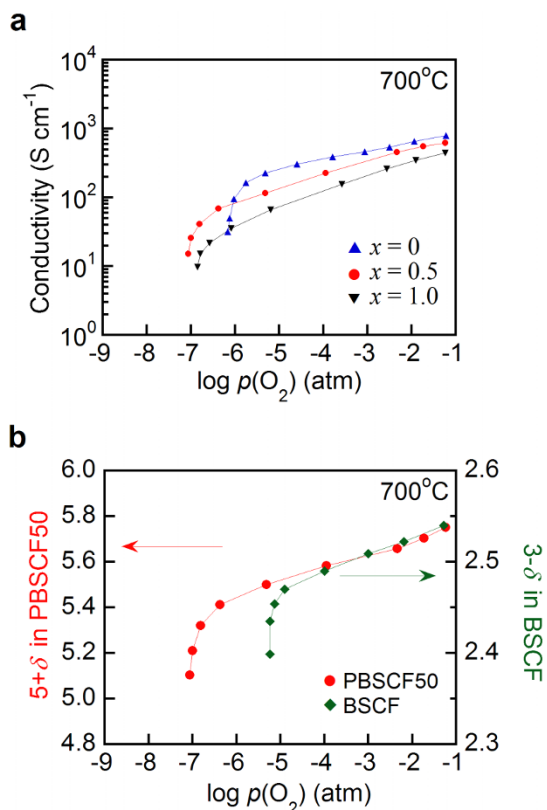


**Figure 2** | Electrical and chemical properties of  $\text{PrBa}_{0.5}\text{Sr}_{0.5}\text{Co}_{2-x}\text{Fe}_x\text{O}_{5+\delta}$  (a) Electrical conductivities of  $\text{PrBa}_{0.5}\text{Sr}_{0.5}\text{Co}_{2-x}\text{Fe}_x\text{O}_{5+\delta}$  ( $x = 0, 0.5,$  and  $1.0$ ) measured at  $700^\circ\text{C}$  in different  $p(\text{O}_2)$ . (b) Oxygen non-stoichiometry of  $\text{PrBa}_{0.5}\text{Sr}_{0.5}\text{Co}_{1.5}\text{Fe}_{0.5}\text{O}_{5+\delta}$  and  $\text{Ba}_{0.5}\text{Sr}_{0.5}\text{Co}_{0.8}\text{Fe}_{0.2}\text{O}_{3-\delta}$  as a function of  $p(\text{O}_2)$  at  $700^\circ\text{C}$ .

samples examined in this study, the electrical conductivities vary from  $10$  to  $10^3 \text{ S cm}^{-1}$  under typical operating conditions, which are sufficient for the cathode application. As  $p(\text{O}_2)$  was decreased below  $\sim 10^{-6} \text{ atm}$  at  $700^\circ\text{C}$ , the conductivity dropped dramatically due to partial reduction of the oxide lattice<sup>24,25</sup>. However, this stability limit can be shifted toward lower  $p(\text{O}_2)$  by increasing the content of Fe doping.

To gain more insight into the redox properties, oxygen nonstoichiometry of the PBSCF05 samples, together with that of BSCF (for comparison), was characterized as a function of  $p(\text{O}_2)$  at  $700^\circ\text{C}$  using coulometric titration (Fig. 2b). The isotherm of ordered PBSCF05 has a lower critical  $p(\text{O}_2)$  for decomposition than that of BSCF, implying that PBSCF05 has higher redox stability or better durability under cathodic polarization, a favourable property for practical SOFC applications.

**Power output and durability of fuel cells.** The electrocatalytic activity for ORR of these materials was determined in symmetrical cells using impedance spectroscopy. The cathodic polarization resistance normalized by the geometric electrode area, the area specific resistance (ASR), can be readily calculated from impedance spectra acquired under open circuit conditions (inset of Fig. 3a). When the electronic conduction in the electrolyte is negligible, the cathodic polarization resistance can be adequately approximated by the diameter of the impedance loop (or the difference between the intersects with the real axis at high and low frequencies); otherwise, it has to be calculated with proper corrections to take into consideration of the partial shorting effect of electronic conduction through the electrolyte<sup>26</sup>. Summarized in Fig. 3a are the ASRs of the  $\text{PrBa}_{0.5}\text{Sr}_{0.5}\text{Co}_{2-x}\text{Fe}_x\text{O}_{5+\delta}$  ( $x = 0, 0.5,$  and  $1.0$ ) electrodes as

determined from impedance spectra. It is noted that, when  $x = 0.5$ , the PBSCF05 showed the lowest ASR in the temperature range studied,  $\sim 0.33 \Omega \text{ cm}^2$  at  $500^\circ\text{C}$  and  $\sim 0.056 \Omega \text{ cm}^2$  at  $600^\circ\text{C}$ , which are lower than those reported for BSCF under similar conditions (e.g.,  $0.7 \Omega \text{ cm}^2$  at  $500^\circ\text{C}$ ). In general, the population of mobile oxygen defects may contribute to the enhanced oxygen kinetics associated with oxygen bulk diffusion and surface exchange<sup>15</sup>. Higher concentration of mobile oxygen defects in the Ln-O layer due to larger amount of Fe doping (up to  $\sim 50\%$ ) may lead to faster oxygen kinetics and better electrochemical performance.

To characterize the performance of these new PBSCF cathode materials in a practical fuel cell, we used anode-supported cells based on a  $\sim 15 \mu\text{m}$  thick GDC electrolyte. Fig. 3b shows some typical  $I$ - $V$  curves and the corresponding power densities of the test cells with PBSCF05-GDC as the cathodes at  $500 \sim 650^\circ\text{C}$ . The peak power densities of the cells were  $0.71, 1.31, 2.16,$  and  $2.90 \text{ W cm}^{-2}$  at  $500, 550, 600,$  and  $650^\circ\text{C}$ , respectively, much higher than those reported for the cells using a BSCF cathode (e.g.,  $1.01 \text{ W cm}^{-2}$  at  $600^\circ\text{C}$ ) which are prepared and tested under similar conditions. Fig. 3c shows the average peak power densities of cells with a cathode of  $\text{LnBa}_{0.5}\text{Sr}_{0.5}\text{Co}_{1.5}\text{Fe}_{0.5}\text{O}_{5+\delta}$  ( $\text{Ln} = \text{Pr}$  and  $\text{Nd}$ )-GDC measured at different operating temperatures. The performance of a Ni-GDC | GDC | PBSCF05-GDC test cell was very stable under a cell voltage of  $0.6 \text{ V}$  at  $550^\circ\text{C}$  for 150 hours (Fig. 3d), demonstrating stable power output without observable degradation.

**DFT prediction of possible elementary pathway for the ORR.** To gain some insight into the structural features of these cathode materials, we performed density functional theory (DFT) calculations<sup>27,28</sup>. Based on our XRD and TEM analyses (Supplementary Table S1 and Fig. 1), we constructed a model for  $\text{PrBa}_{0.5}\text{Sr}_{0.5}\text{Co}_{1.5}\text{Fe}_{0.5}\text{O}_{6.0}$  (PBSCFO6.0) (Supplementary Fig. S10). Calculations of oxygen-vacancy formation energy ( $E_{\text{OV}}$ ) in this model suggest that it is energetically more favorable to form oxygen vacancies in the vicinity of Co ions than that of Fe ions (Supplementary Fig. S11 and Table S3;  $E_{\text{OV}} = 1.18 \text{ eV}$  versus  $1.36 \text{ eV}$ ). When two oxygen ions connected to the Co ion are removed, it reduces to  $\text{PrBa}_{0.5}\text{Sr}_{0.5}\text{Co}_{1.5}\text{Fe}_{0.5}\text{O}_{5.875}$  (PBSCFO5.875), forming a pore channel (Supplementary Fig. S12). However, we found that the activation energy for oxygen diffusion through the channel in PBSCFO5.875 is  $\sim 2.6 \text{ eV}$ , which is much higher than the experimental values ( $\sim 0.55 \text{ eV}$ ). To lower the reaction barrier, more oxygen ions connected to the Co ions were removed (Supplementary Fig. S12). Based on our DFT modeling results, several types of pore channels (Fig. 4a) could be proposed for the defective structures; one of the oxygen ion diffusion paths may follow a zig-zag type trajectory through the CoO plane perpendicular to the PrO plane (Fig. 4b), because the reaction barrier ( $\sim 0.46 \text{ eV}$ ) for  $\text{PrBa}_{0.5}\text{Sr}_{0.5}\text{Co}_{1.5}\text{Fe}_{0.5}\text{O}_{5.75}$  (PBSCFO5.75) and  $\text{PrBa}_{0.5}\text{Sr}_{0.5}\text{Co}_{1.5}\text{Fe}_{0.5}\text{O}_{5.625}$  (PBSCFO5.625) is closer to the experimental value ( $\sim 0.55 \text{ eV}$ ).

Further, a 2-D surface model was also constructed to simulate the interactions between  $\text{O}_2$  and the PBSCO(010) surface (Supplementary Fig. S13 and S14). DFT calculations suggest that the most probable elementary pathway for the ORR on the PBSCFO cathode can be described as follows (Fig. 4b and Supplementary Table S4): (1) adsorption and dissociation of molecular  $\text{O}_2$  on an oxygen vacancy near a Co ion, (2) incorporation of the dissociated oxygen ions into the pore channels; (3) diffusion of the oxygen ions through the pore channels (bulk diffusion), and (4) combination of the oxygen ions with oxygen vacancies in the GDC electrolyte.

## Discussion

In conclusion, a class of cation-ordered, double-perovskite compounds display fast oxygen ion diffusion through pore channels and high catalytic activity toward ORR at low temperatures while maintaining excellent compatibility with electrolyte and good

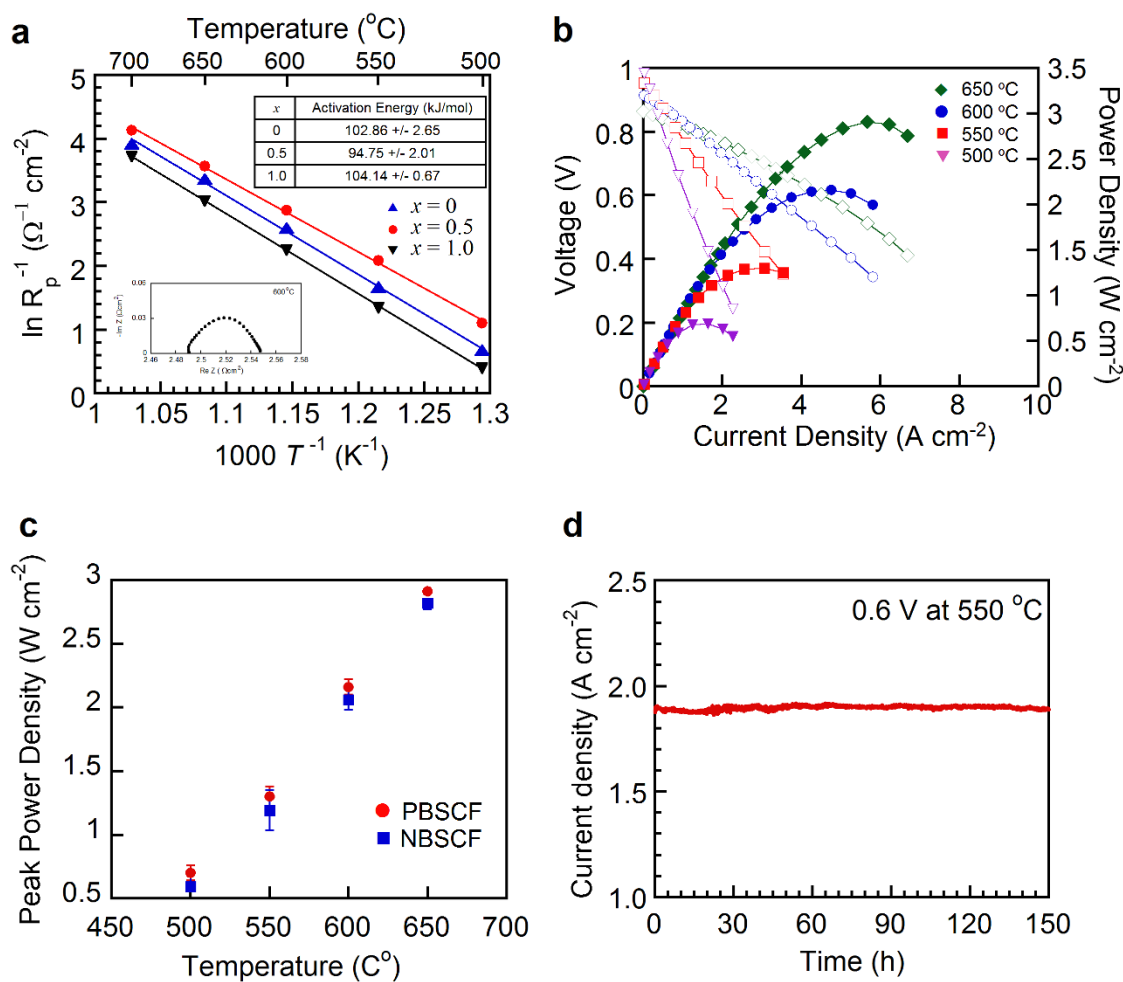


**Figure 3** | Electrochemical properties of  $\text{PrBa}_{0.5}\text{Sr}_{0.5}\text{Co}_{2-x}\text{Fe}_x\text{O}_{5+\delta}$  in fuel cells (a) Arrhenius plot of reciprocal ASR for  $\text{PrBa}_{0.5}\text{Sr}_{0.5}\text{Co}_{2-x}\text{Fe}_x\text{O}_{5+\delta}$ -GDC ( $x = 0, 0.5,$  and  $1.0$ ) cathode. The inset shows the ASR of PBSCF05-GDC cathode measured at  $600^\circ\text{C}$  in air under open-circuit conditions. (b)  $I$ - $V$  curves and the corresponding power densities of test cells with PBSCF05-GDC cathode using humidified  $\text{H}_2$  (3%  $\text{H}_2\text{O}$ ) as the fuel and ambient air as the oxidant to the cathode at  $500 \sim 650^\circ\text{C}$ . (c) Peak power densities of cells with  $\text{LnBa}_{0.5}\text{Sr}_{0.5}\text{Co}_{1.5}\text{Fe}_{0.5}\text{O}_{5+\delta}$ -GDC ( $\text{Ln} = \text{Pr}$  and  $\text{Nd}$ ) cathode. (d) Short term stability measurement for a test cell, Ni-GDC | GDC | PBSCF05-GDC, at a constant cell voltage of  $0.6 \text{ V}$  at  $550^\circ\text{C}$ .

stability under typical fuel cell operating conditions. DFT analysis using simplified models suggests that the most attractive properties of these materials are the pore channels in the [PrO] and [CoO] planes that could provide fast paths for oxygen transport, which in turn accelerates the kinetics of surface oxygen exchange. More detailed understanding of the mechanistic details may help to rationally design better double-perovskite cathode materials for a new generation of high-performance SOFCs with enhanced durability.

## Methods

**Synthesis of electrode and electrolyte powders.** Cathode materials  $\text{LnBa}_{0.5}\text{Sr}_{0.5}\text{Co}_{2-x}\text{Fe}_x\text{O}_{5+\delta}$  (LnBSCF) ( $\text{Ln} = \text{Pr}$  and  $\text{Nd}$ ;  $x = 0, 0.25, 0.5, 0.75,$  and  $1.0$ ) were synthesized using a glycine-nitrate process (GNP). Stoichiometric amounts of  $\text{Ln}(\text{NO}_3)_3 \cdot 6\text{H}_2\text{O}$  (Aldrich, 99.9%, metal basis),  $\text{Ba}(\text{NO}_3)_2$  (Aldrich, 99+%),  $\text{Sr}(\text{NO}_3)_2$  (Aldrich, 99+%),  $\text{Co}(\text{NO}_3)_2 \cdot 6\text{H}_2\text{O}$  (Aldrich, 98+%), and  $\text{Fe}(\text{NO}_3)_3 \cdot 6\text{H}_2\text{O}$  (Aldrich, 98%) were dissolved in distilled water with proper amount of glycine. The solutions were heated up to  $350^\circ\text{C}$  in air and followed by combustion to form fine powders, which were calcined at  $600^\circ\text{C}$  for 4 hours. The resulting powders were then grinded and calcined again at  $900^\circ\text{C}$  for 4 hours. For the measurement of electrical conductivity and coulometric titration, the powders were pressed into pellets at 5 MPa and sintered in air at  $1100 \sim 1150^\circ\text{C}$  for 12 hours (to achieve relative density > 97%). For transmission electron microscopy (TEM), the  $\text{PrBa}_{0.5}\text{Sr}_{0.5}\text{Co}_{1.5}\text{Fe}_{0.5}\text{O}_{5+\delta}$  (PBSCF05) sample was annealed at  $700^\circ\text{C}$  for 600 hours. The  $\text{Ce}_{0.9}\text{Gd}_{0.1}\text{O}_{2-\delta}$  (GDC) powders for electrolyte and NiO-GDC powders for anode were also synthesized using the GNP method. For preparation of cathode slurries, pre-calcined cathode and GDC powders (at a weight ratio of 60 : 40) were mixed using ball milling, together with an organic binder (Heraeus V006).

**Fabrication of fuel cells and TEM sample preparation.** Symmetrical cells with a configuration of electrode | GDC | electrode were used for impedance spectroscopy. GDC powder was pressed into pellets of  $\sim 1 \text{ mm}$  thick and sintered at  $1350^\circ\text{C}$  for 4 hours in air to obtain a dense electrolyte membrane. Cathode slurries were then painted onto both surfaces of dense GDC electrolyte and fired at  $950^\circ\text{C}$  for 4 hours. Ni-GDC anode-supported cells with a configuration of Ni-GDC | GDC | cathode were fabricated using a drop-coating method. NiO powder, GDC powder, and starch (weight ratio of 6 : 4 : 1.5) were mixed using ball milling in ethanol for 24 hours. After drying, the NiO-GDC mixture was pressed into a pellet ( $\sim 0.6 \text{ mm}$  thick and  $15 \text{ mm}$  diameter). Thin GDC electrolyte membranes were prepared by a refined particle suspension coating technique. A GDC suspension was prepared by dispersing GDC powders (Aldrich) in ethanol with a small amount of binder (polyvinyl Butyral, B-98) and dispersant (Triethanolamine, Alfa Aesar) at a ratio of 1 : 10. The GDC suspension was applied to a NiO-GDC anode support by drop-coating, followed by drying in air and subsequent co-sintering at  $1400^\circ\text{C}$  for 5 hours. Cross-sectional samples for TEM analysis were prepared using a focused ion beam (FIB, Quanta 3D, FEI).

**Electrical and electrochemical testing.** Electrical conductivities of the LnBSCF cathode materials were determined in air using a four-electrode measurement. All four electrodes were made of Ag wire and Ag paste. The current and voltage were controlled/measured using a potentiostat (BioLogic) in the temperature range of  $100$  to  $750^\circ\text{C}$  with an interval of  $50^\circ\text{C}$ .

For symmetrical cells, two Ag wires were attached to each of the two electrodes using Ag paste. Each cell was mounted on an alumina tube using a ceramic adhesive (Aremco, Ceramabond 552). Impedance spectra were recorded under OCV in a frequency range of  $1 \text{ mHz}$  to  $500 \text{ kHz}$  with ac perturbation of  $10 \text{ mA}$  in the temperature range of  $500 \sim 650^\circ\text{C}$ . For the single cell tests, each cell was mounted on an alumina tube using a ceramic adhesive. Humidified (with 3 v%  $\text{H}_2\text{O}$ )  $\text{H}_2$  was used as the fuel at a flow rate of  $100 \text{ mL min}^{-1}$  (passing through a water bubbler at  $25^\circ\text{C}$ ), whereas ambient air was supplied to cathode as the oxidant. Impedance spectra and

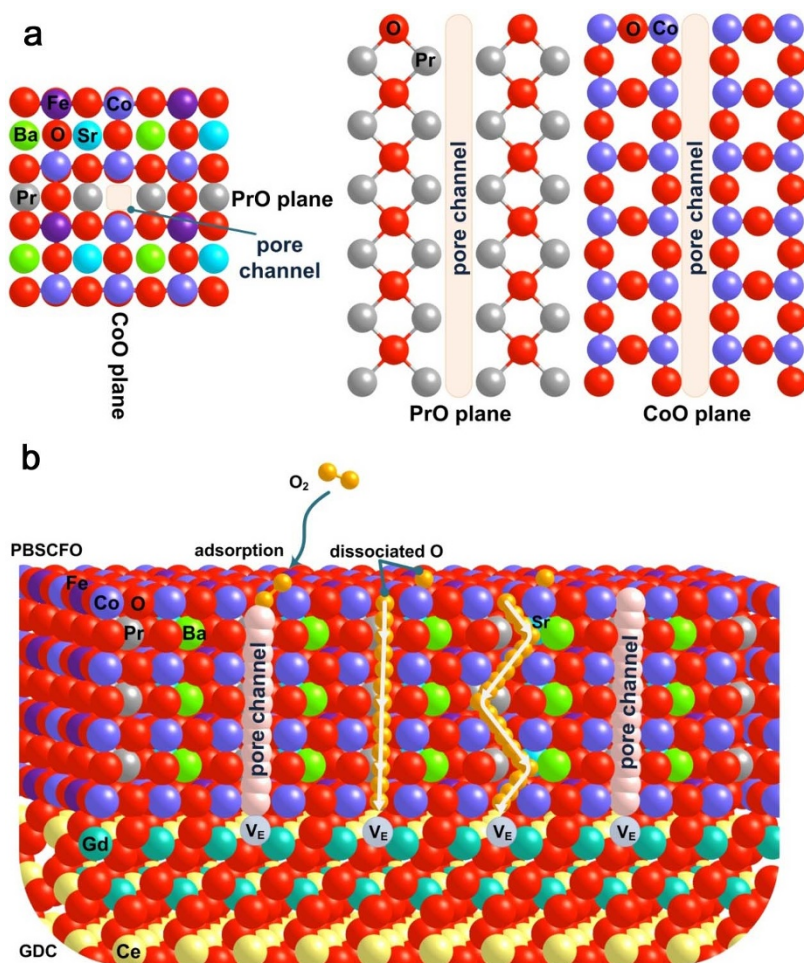


**Figure 4** | DFT calculations for elucidating the most probable elementary pathway for the ORR on the PBSCFO (a) Schematic illustration of PBSCFO with a pore channel labeled with a round box on the (010) plane. To illustrate the pore channel through the PrO plane and the CoO plane (perpendicular to the PrO plane), only the PrO and the CoO layers were shown. (b) A proposed mechanism for the surface ORR and the bulk diffusion via the pore channels in  $\text{PrBa}_{0.5}\text{Sr}_{0.5}\text{Co}_{2-x}\text{Fe}_x\text{O}_{5+\delta}$  (010).  $V_E$  is an oxygen vacancy in the GDC electrolyte.

$I$ - $V$  polarization curves were obtained with a BioLogic Potentiostat. The  $I$ - $V$  polarization curves were recorded between 500 °C and 650 °C.

**Redox property and oxygen nonstoichiometric.** The redox properties and oxygen nonstoichiometry of LnBSCF cathodes and  $\text{Ba}_{0.5}\text{Sr}_{0.5}\text{Co}_{0.8}\text{Fe}_{0.2}\text{O}_{3-\delta}$  (BSCF) were measured using coulometric titration (CT) as a function of the oxygen partial pressure,  $p(\text{O}_2)$ . The detailed CT procedure is as described elsewhere<sup>24,25</sup>. After purging 5%  $\text{O}_2$ -Ar gas over the sample in the tube for 24 hours,  $p(\text{O}_2)$  was determined from the OCV. The sample was allowed to equilibrate with the surrounding atmosphere until the change in potential was less than 1 mV h<sup>-1</sup>. Oxygen nonstoichiometry was determined through this procedure at 700 °C over a wide range of oxygen partial pressure. Electrical conductivity was measured using a four-electrode configuration and a BioLogic Potentiostat.

**DFT calculation.** The Vienna *ab initio* simulation package (VASP)<sup>27,29</sup> was used for periodic density functional theory (DFT) calculations. As reported<sup>28</sup>, it is difficult to apply for the DFT + U approach since the concurrent optimization of two  $U_{\text{eff}}$  parameters of two B-site cations of  $\text{PrBa}_{0.5}\text{Sr}_{0.5}\text{Co}_{2-x}\text{Fe}_x\text{O}_{5+\delta}$  (PBSCFO) is problematic. Thus in this study, we carried out the spin-polarization method with the generalized gradient approximation (GGA) with the projector-augmented-wave method (PAW)<sup>30</sup> using the Perdew-Burke-Ernzerhof (PBE) exchange-correlation functional. To simulate the oxygen-deficient double perovskite PBSCFO, we constructed a tetragonal  $P4/mmm$  structure ( $a = b \neq c$ ). The kinetic energy cutoff for a plane wave basis set was 415 eV. The Brillouin zone was sampled with the  $(3 \times 3 \times 3)$  and  $(3 \times 3 \times 1)$  Monkhorst-Pack mesh  $k$ -points<sup>31</sup> for bulk and surface calculations. For the 2-D surface calculations, the slabs were separated by a vacuum space of 15 Å in the direction perpendicular to the surface. In this study, the adsorption energy ( $E_{\text{ad}}$ ) on a CoFeO(010)-terminated surface (1/16 ML) was calculated by  $E_{\text{ad}} = E[\text{O-PBSCFO}] - E[\text{PBSCFO}] - 1/2E[\text{O}_2]$ , where  $E[\text{O-PBSCFO}]$ ,  $E[\text{PBSCFO}]$ , and  $E[\text{O}_2]$  are the predicted electronic energies for an adsorbed O species on a PBSCFO surface, a bare PBSCFO surface, and a gas-phase triplet  $\text{O}_2$ , respectively. The oxygen-vacancy formation energy ( $E_{\text{OV}}$ )<sup>28,32</sup> was calculated by  $E_{\text{OV}} = E[\text{defective PBSCFO}] + 1/$

$2E[\text{triplet O}_2] - E[\text{perfect PBSCFO}]$ , where  $E[\text{defective PBSCFO}]$  and  $E[\text{perfect PBSCFO}]$  are the predicted electronic energies for defective and perfect bulk PBSCFO structures, respectively.

**Other Characterization.** X-ray powder diffraction (XRD) (Rigaku diffractometer, Cu K $\alpha$  radiation) analysis was used to confirm the crystalline structures of samples. In situ XRD was obtained from room to operating temperature (Bruker, D8 Advance). The microstructures and morphologies of LnBSCF cathode samples were observed using a field emission scanning electron microscope (SEM) (Nova SEM). The TEM images were acquired with JEOL JEM 2100F with a probe forming (STEM) Cs corrector at 200 kV. A thermogravimetric analysis (TGA) was carried out using a SDT-Q600 (TA instrument, USA). TGA experiments were performed from 100 °C to 900 °C with a heating/cooling rate of 2 °C min<sup>-1</sup> in air. The room-temperature oxygen content values were determined by iodometric titration.

1. Singhal, S. C. Advances in solid oxide fuel cell technology. *Solid State Ionics* **135**, 305–313 (2000).
2. Park, S. D., Vohs, J. M. & Gorte, R. J. Direct oxidation of hydrocarbons in a solid-oxide fuel cell. *Nature* **404**, 265–267 (2000).
3. Tao, S. & Irvine, J. T. S. A redox-stable efficient anode for solid-oxide fuel cells. *Nat. Mater.* **2**, 320–323 (2003).
4. Shin, T. H., Ida, S. & Ishihara, T. Doped  $\text{CeO}_2$ -LaFeO<sub>3</sub> Composite Oxide as an Active Anode for Direct Hydrocarbon-Type Solid Oxide Fuel Cells. *J. Am. Chem. Soc.* **133**, 19399–19407 (2011).
5. Liu, M., Lynch, M. E., Blinn, K., Alamgir, F. M. & Choi, Y. Rational SOFC material design: new advances and tools. *Mater. Today* **14**, 534–546 (2011).
6. Yang, L., Wang, S. Z., Blinn, K., Liu, M., Liu, Z., Cheng, Z. & Liu, M. Enhanced Sulfur and Coking Tolerance of a Mixed Ion Conductor for SOFCs:  $\text{BaZr}_{0.1}\text{Ce}_{0.7}\text{Y}_{0.2-x}\text{Yb}_x\text{O}_{3-\delta}$ . *Science* **326**, 126–129 (2009).
7. Yang, L. *et al.* Promotion of water-mediated carbon removal by nanostructured barium oxide/nickel interfaces in solid oxide fuel cells. *Nat. Commun.* **2** (2011).



8. Mogensen, M., Jensen, K. V., Jørgensen, M. J. & Primdahl, S. Progress in understanding SOFC electrodes. *Solid State Ionics* **150**, 123–129 (2002).
9. Wachman, E. D. & Lee, K. T. Lowering the temperature of solid oxide fuel cells. *Science* **334**, 935–939 (2011).
10. Steele, B. C. H. Material science and engineering: The enabling technology for the commercialisation of fuel cell systems. *J. Mater. Sci.* **36**, 1053–1068 (2001).
11. Fleig, J. Solid oxide fuel cell cathodes: Polarization mechanisms and modeling of the electrochemical performance. *Annu. Rev. Mater. Res.* **33**, 361–382 (2003).
12. Xia, C., Rauch, W., Chen, F. & Liu, M.  $\text{Sm}_{0.5}\text{Sr}_{0.5}\text{CoO}_3$  cathodes for low-temperature SOFCs. *Solid State Ionics* **149**, 11–19 (2002).
13. Shao, Z. & Haile, S. M. A high-performance cathode for the next generation of solid-oxide fuel cells. *Nature* **431**, 170–173 (2004).
14. Finsterbusch, M., Lussier, A., Schaefer, J. A. & Idzerda, Y. U. Electrochemically driven cation segregation in the mixed conductor  $\text{La}_{0.6}\text{Sr}_{0.4}\text{Co}_{0.2}\text{Fe}_{0.8}\text{O}_{3-\delta}$ . *Solid State Ionics* **12**, 77–80 (2012).
15. Kim, G. *et al.* Rapid oxygen ion diffusion and surface exchange kinetics in  $\text{PrBaCo}_2\text{O}_{5+x}$  with a perovskite related structure and ordered A cations. *J. Mater. Chem.* **17**, 2500–2505 (2007).
16. Jacobson, A. J. Materials for solid oxide fuel cells. *Chem. Mater.* **22**, 660–674 (2010).
17. Tarcón, A., Skinner, S. J., Chater, R. J., Hernández-Ramírez, F. & Kilner, J. A. Layered perovskites as promising cathodes for intermediate temperature solid oxide fuel cell. *J. Mater. Chem.* **17**, 3175–3181 (2007).
18. Taskin, A. A., Lavrov, A. N. & Ando, Y. Achieving fast oxygen diffusion in perovskites by cation ordering. *Appl. Phys. Lett.* **86**, 091910–091913 (2005).
19. Kim, J.-H. & Manthiram, A.  $\text{LnBaCo}_2\text{O}_{5+\delta}$  oxide as cathodes for intermediate-temperature solid oxide fuel cells. *J. Electrochem. Soc.* **155**(4), B385–B390 (2008).
20. Kim, J. H., Cassidy, M., Irvine, J. T. S. & Bae, J. Electrochemical investigation of composite cathodes with  $\text{SmBa}_{0.5}\text{Sr}_{0.5}\text{Co}_2\text{O}_{5+\delta}$  cathodes for intermediate temperature-operating solid oxide fuel cell. *Chem. Mater.* **22**, 883–892 (2010).
21. Chen, D., Ran, R., Zhang, K., Wang, J. & Shao, Z. Intermediate-temperature electrochemical performance of a polycrystalline  $\text{PrBaCo}_2\text{O}_{5+\delta}$  cathode on samarium-doped ceria electrolyte. *J. Power Sources* **188**, 96–105 (2009).
22. Lynch, M. E. *et al.* Enhancement of  $\text{La}_{0.6}\text{Sr}_{0.4}\text{Co}_{0.2}\text{Fe}_{0.8}\text{O}_{3-\delta}$  durability and surface electrocatalytic activity by  $\text{La}_{0.85}\text{Sr}_{0.15}\text{MnO}_{3\pm\delta}$  investigated using a new test-electrode platform. *Energy Environ. Sci.* **4**, 2249–2258 (2011).
23. Bastidas, D. M., Tao, S. & Irvine, J. T. S. A symmetrical solid oxide fuel cell demonstrating redox stable perovskite electrodes. *J. Mater. Chem.* **16**, 1603–1605 (2006).
24. Yoo, S., Shin, J. & Kim, G. Thermodynamic and electrical characteristics of  $\text{NdBaCo}_2\text{O}_{5+\delta}$  at various oxidation and reduction states. *J. Mater. Chem.* **21**, 493–443 (2011).
25. Yoo, S., Choi, S., Shin, J., Liu, M. & Kim, G. Electrical properties, thermodynamic behavior, and defect analysis of  $\text{La}_{m+1}\text{Ni}_m\text{O}_{3n+1+\delta}$  infiltrated into YSZ scaffolds as cathodes for intermediate-temperature SOFCs. *RSC Adv.* **2**, 4648–4655 (2012).
26. Hu, H. & Liu, M. Effect of interfacial resistance on determination of transport properties of mixed-conducting electrolytes. *J. Electrochem. Soc.* **143**(6), L109–L112 (1996).
27. Kresse, G. & Furthmüller, J. Efficient iterative schemes for *ab initio* total-energy calculations using a plane-wave basis set. *Phys. Rev. B* **54**, 11169–11186 (1996).
28. Mastrokov, Y. A., Kuklja, M. M., Kotomin, E. A. & Maier, J. First-principles modelling of complex perovskite  $(\text{Ba}_{1-x}\text{Sr}_x)(\text{Co}_{1-y}\text{Fe}_y)\text{O}_{3-\delta}$  for solid oxide fuel cell and gas separation membrane applications. *Energy Environ. Sci.* **3**, 1544–1550 (2010).
29. Kresse, G. & Hafner, J. *Ab initio* molecular dynamics for liquid metals. *Phys. Rev. B* **47**, 558–561 (1993).
30. Blöchl, P. E. Projector augmented-wave method. *Phys. Rev. B* **50**, 17953–17979 (1994).
31. Monkhorst, H. J. & Pack, J. D. Special points for Brillouin-zone integrations. *Phys. Rev. B* **13**, 5188–5192 (1976).
32. Choi, Y., Lin, M. C. & Liu, M. Rational design of novel cathode materials in solid oxide fuel cells using first-principles simulations. *J. Power Sources* **195**, 1441–1445 (2010).

## Acknowledgements

This research was supported by WCU (World Class University) program (R31-2009-000-20012-0) and Mid-career Researcher Program (2011-0010773) through the National Research Foundation of Korea, funded by the Ministry of Education, Science and Technology, and the New & Renewable Energy of the Korea Institute of Energy Technology Evaluation and Planning (KETEP) grant (20113020030060) funded by the Korea government Ministry of Knowledge Economy. DFT calculations were performed at the National Energy Research Scientific Computing Center (Contract No. DE-AC02-05CH11231) and KAUST Supercomputing Laboratory.

## Author contributions

S.C., S.Y., J.K., S.P., A.J., S.S. and J.K. fabricated samples and carried out analytical and electrochemical characterizations. H.Y.J. collected and analyzed the TEM data. Y.C. performed the DFT calculations. All authors contributed to writing the paper. J.S., G.K. and M.L. conceived and coordinated the project.

## Additional information

**Supplementary information** accompanies this paper at <http://www.nature.com/scientificreports>

**Competing financial interests:** The authors declare no competing financial interests.

**How to cite this article:** Choi, S. *et al.* Highly efficient and robust cathode materials for low-temperature solid oxide fuel cells:  $\text{PrBa}_{0.5}\text{Sr}_{0.5}\text{Co}_{2-x}\text{Fe}_x\text{O}_{5+\delta}$ . *Sci. Rep.* **3**, 2426; DOI:10.1038/srep02426 (2013).



This work is licensed under a Creative Commons Attribution-NonCommercial-NoDerivs 3.0 Unported license. To view a copy of this license, visit <http://creativecommons.org/licenses/by-nc-nd/3.0>